ELSEVIER

Journal of Hydrology 259 (2002) 15–31

Journal of Hydrology

www.elsevier.com/locate/jhydrol

Calibration of Richards' and convection–dispersion equations to field-scale water flow and solute transport under rainfall conditions

Diederik Jacques[a,*], Jirka Šimůnek[b], Anthony Timmerman[a], Jan Feyen[a]

[a]*Institute for Land and Water Management, Katholieke Universiteit Leuven, Vital Decosterstraat 102, 3000 Leuven, Belgium*
[b]*George E. Brown Jr Salinity Laboratory, USDA-ARS, 450 W. Big Springs Road, Riverside, CA 92507, USA*

Received 21 July 2000; revised 30 October 2001; accepted 12 November 2001

Abstract

In this paper, the applicability of Richards' equation for water flow and the convection–dispersion equation for solute transport is evaluated to model field-scale flow and transport under natural boundary conditions by using detailed experimental data and inverse optimization. The data consisted of depth-averaged time series of water content, pressure head and resident solute concentration data measured several times a day during 384 d. In a first approach, effective parameters are estimated using the time series for one depth and assuming a homogeneous soil profile. In a second approach, all time series were used simultaneously to estimate the parameters of a multi-layered soil profile. Water flow was described by the Richards' equation and solute transport either by the equilibrium convection–dispersion (CDE) or the physical non-equilibrium convection–dispersion (MIM) equation. To represent the dynamics of the water content and pressure head data, the multi-layered soil profile approach gave better results. Fitted soil hydraulic parameters were comparable with parameters obtained with other methods on the same soil. At larger depths, both the CDE- and MIM-models gave acceptable descriptions of the observed breakthrough data, although the MIM performed somewhat better in the tailing part. Both models underestimated significantly the fast breakthrough. To describe the breakthrough curves at the first depth, only the MIM with a mixing layer close to the soil surface gave acceptable results. Starting from an initial value problem with solutes homogeneously distributed over the mobile and immobile water phase was preferable compared to the incorporation of a small layer with only mobile water near the soil surface.

Keywords: Parameter optimization; Numerical modeling; Unsaturated zone; Water and solute transport

1. Introduction

The Richards' equation for water flow and the convection–dispersion equation (CDE) for solute transport are frequently used to describe water and solute transport experiments in undisturbed soil columns and field soils (e.g. Schulin et al., 1987; Butters and Jury, 1989; Roth et al., 1991; Flury, 1993; Radcliffe et al., 1996). Sometimes, however, significant differences are observed between observations and the results of model calculations such as higher measured concentrations at the beginning of the solute breakthrough or tailing (e.g. Snow et al., 1994; Jacques et al., 1998) which is especially the case in structured or macroporous soils. An alternative is the non-equilibrium convection–dispersion equation to describe solute transport in such structured soils (e.g. Jacobsen et al., 1992; Mallants, 1996; Schoen et al., 1999; Vanderborght et al., 2000).

* Corresponding author. Address: SCK.CEN, Studiecentrum voor Kernenergie, Waste and Disposal, Boeretang 200, 2400 Mol, Belgium. Tel.: +32-14-333-209; fax: +32-14-323-553.
E-mail address: djacques@sckcen.be (D. Jacques).

0022-1694/02/$ - see front matter
PII: S0022-1694(01)00591-1

However, a throughout evaluation of models based on Richards' equation and the (non-) equilibrium convection–dispersion equation to describe water flow and solute transport under transient field conditions is still limited, mainly because detailed experimental data at that scale are scarce. A strict evaluation of the processes described by a model should be done using independent experimentally obtained parameters. For some parameters, however, no techniques are available to measure them at the field-scale. Alternatively, models are calibrated using measured variables (such as water content, solute concentration, fluxes) to obtain a set of model parameters able to reproduce the measurements, also called inverse optimization. The calibrated model is then evaluated by judging its ability to predict the dynamics of the states variables for different initial and boundary conditions or for other state variables (e.g. resident versus flux concentrations, Vanderborght et al., 2000). When detailed (in time and/or space) measurements of (several) variables are available, it is possible to perform an evaluation of a conceptual or mathematical model based on how good the model reproduces the dynamics of the measurements and a physical interpretation of the fitted parameters.

In general, a relatively large amount of model parameters has to be estimated since most soil profiles consist of soil layers having different properties. For each soil layer, the interaction between water content, pressure head, and unsaturated hydraulic conductivity has to be determined. Instead of using a 'subjective' trial and error approach, more objective and/or automated algorithms are used to estimate soil hydraulic parameters in multi-layered soils (Lehman and Ackerer, 1997; Kasteel, 1997; Abbaspour et al., 1999, 2000), solute transport parameters under natural boundary conditions (e.g. Ventrella et al., 2000) and coupled estimation of flow and solute transport parameters for ground water flow problems (e.g. Mishra and Parker, 1989; Sun and Yeh, 1990; Medina and Carrera, 1996; Mayer and Huang, 1999). However, studies simultaneously estimating water flow and solute transport parameters for transient variably-saturated media are less common (e.g. Inoue et al., 2000), especially in a layered soil-profile and for field conditions.

The main objectives of the paper were to evaluate the applicability of Richards' equation and the equilibrium or non-equilibrium convection dispersion equation to describe field-scale water flow and solute transport in a layered soil profile under natural rainfall boundary conditions and to determine simultaneously soil hydraulic and solute transport parameters for different horizons. The evaluation is based on the combination detailed measurements of time series of water content, pressure heads, and solute concentration, an semi-automatic inverse optimization technique, and a numerical model.

2. Theory

2.1. Water flow model

In this study, one-dimensional vertical water flow in variably-saturated porous medium is described using Richards' equation:

$$\frac{\partial \theta}{\partial t} = \frac{\partial}{\partial z}\left(K(\psi)\frac{\partial \psi}{\partial z}\right) - \frac{\partial K(\psi)}{\partial z} \tag{1}$$

where θ is the volumetric water content [L^3L^{-3}], t the time [T], z the vertical coordinate (positive downwards) [L], ψ the pressure head [L], and K the hydraulic conductivity [LT^{-1}]. The upper boundary condition is defined here as an atmospheric condition. Under this condition, water infiltration corresponds to hourly rainfall rates as long as there is no ponding of water at the soil surface. Surplus of water is assumed to be removed by run-off. Also, note that we neglect evaporation since it was assumed that it is negligible during the experiment due to the presence of a thin layer of gravel (see Section 3). The lower boundary is defined as a zero pressure head gradient, i.e. free drainage. The initial condition is given as a linear interpolation of the measured pressure heads between the five depths at day 0.

We used the empirical model of van Genuchten (1980) to describe the water retention characteristic, $\theta(\psi)$:

$$\theta = \frac{(\theta_s - \theta_r)}{(1 + |\alpha\psi|^n)^m} + \theta_r \qquad (\psi \le 0) \tag{2}$$

where θ_r and θ_s [L^3L^{-3}] are the residual and the saturated water content, respectively, α [L^{-1}], n, and m [–] are shape parameters. Combined with the statistical pore-size distribution model for the

unsaturated hydraulic conductivity of Mualem (1976) and the restriction $m = 1 - 1/n$, an analytical model for the hydraulic conductivity curve, $K(\psi)$, becomes (van Genuchten, 1980):

$$K(\psi) = K_s \frac{\left|1 - (\alpha|\psi|)^{mn}(1 + (\alpha|\psi|)^n)^{-m}\right|^2}{[1 + (\alpha|\psi|)^n]^{ml}} \quad (\psi \leq 0) \tag{3}$$

where K_s [LT^{-1}] is the saturated hydraulic conductivity, and l the pore connectivity and tortuosity factor [–]. A preliminary analysis showed that θ_r did not influence the simulated time series of θ and ψ for the experimental conditions and was fixed at 0.078 which is the average value for a loamy soil as given by Carsel and Parrish (1988). Therefore, the vector of unknown parameters of the soil hydraulic functions contains five unknowns and is denoted as $\mathbf{b}_h = \{\theta_s, \alpha, n, K_s, l\}$, in this paper.

2.2. Solute transport model

In this paper, the equilibrium convection–dispersion equation (denoted as CDE throughout the paper) represents a first model, while the physical non-equilibrium convection–dispersion equation, also called the mobile–immobile model (MIM), represents a second model. The mathematical representation of the CDE for a non-sorbing, conservative solute is:

$$\frac{\partial \theta C}{\partial t} = \frac{\partial}{\partial z}\left(\theta D \frac{\partial C}{\partial z}\right) - \frac{\partial v \theta C}{\partial z} \tag{4}$$

where C is the solute concentration [ML^{-3}], D the dispersion coefficient [L^2T^{-1}], and v the average pore water velocity [LT^{-1}]. The dispersion coefficient is defined as (ignoring molecular diffusion):

$$D = \lambda|v| \tag{5}$$

where λ is the dispersivity [L]. The dispersivity is viewed as a material constant independent of the flow rate. Since v is obtained from the numerical solution of the water flow model (the water flux q [LT^{-1}] divided by θ), the vector of unknown parameters for the CDE-model, $\mathbf{b}_{se}$, contains only λ.

In the MIM-model, it is assumed that a part of the liquid phase is immobile and is not available for convective transport. However, solutes can be exchanged between the mobile and immobile regions by means of a first-order exchange process. The mathematical formulation of the MIM for transient water flow for a non-sorbing, conservative trancer is (van Genuchten and Wierenga, 1976):

$$\frac{\partial \theta_m C_m}{\partial t} + \frac{\partial \theta_{im} C_{im}}{\partial t} = \frac{\partial}{\partial z}\left(\theta_m D \frac{\partial C_m}{\partial z}\right) - \frac{\partial v \theta_m C_m}{\partial z} \tag{6}$$

$$\frac{\partial \theta_{im} C_{im}}{\partial t} = \omega(C_m - C_{im}) \tag{7}$$

where θ_m and θ_{im} are the mobile and immobile water contents, respectively, C_m and C_{im} the resident solute concentrations in the mobile and immobile regions, respectively, and ω the first-order exchange coefficient [T^{-1}]. Note that v is the average pore water flux in the mobile region, thus $v = q/\theta_m$. Three unknown parameters should be estimated for the MIM transport model, i.e. $\mathbf{b}_{sne} = \{\lambda, \theta_{im}, \omega\}$. The upper solute transport boundary condition was defined as a Cauchy boundary condition (Šimůnek et al., 1998). Details are given below (see Section 3). A zero solute concentration gradient was assumed as the lower solute transport boundary condition. No solute was present at the beginning of the simulation.

2.3. Formulation of the inverse problem

During the inverse procedure, the unknown parameter vectors are optimized by minimizing a given objective function. The objective function is defined here as (Šimůnek et al., 1998):

$$\Phi(\mathbf{g}; \mathbf{b}|\mathbf{c}) = \sum_{j=1}^{m}\left\{v_j \sum_{i=1}^{n_j} w_{ij}\left[g_j^*(t_i) - g_j(t_i, \mathbf{b}|\mathbf{c})\right]^2\right\} \tag{8}$$

where n_j is the number of observations for the jth measurement set, $\mathbf{g}$ the vector containing the measured values (see below), $\mathbf{b}|\mathbf{c}$ the vector $\mathbf{b}$ containing the unknown parameters estimated given the fixed and known parameters in vector $\mathbf{c}$, m the number of parameter sets, $g_j^*(t_i)$ the measured variable at time t_i for the jth measurement set, $g_j(t_i, \boldsymbol{b}|\boldsymbol{c})$ the corresponding model prediction, and v_j and w_{ij} are the weights for the jth measurement set and the individual observations, respectively. In this study, each w_{ij} is assumed

Table 1
Average soil textures measured at different depths in the trench

Depth (cm)	No of samples	> 50 μm (%)	50–20 μm (%)	20–10 μm (%)	10–2 μm (%)	< 2 μm (%)
15	7	58.6	19.3	6.4	4.5	11.1
35	8	56.7	18.9	7.8	3.2	13.3
55	5	57.3	17.6	6.6	3.7	14.8
75	3	49.6	21.2	7.9	4.4	17.4
95	4	43.8	30.03	7.4	4.5	14

to be equal to 1 and v_j is given by:

$$v_j = \frac{1}{n_j \sigma_j^2} \tag{9}$$

where σ_j^2 is the measurement variances for the jth measurement set. This formulation of the inverse problem is similar to those of Šimůnek et al. (1999, 2000) and Inoue et al. (2000). The Hydrus-1D code (Šimůnek et al., 1998) was used for the numerical solution of the governing equations and the non-linear parameter optimization. The algorithm proposed by Marquardt (1963) is used here to minimize the objective function (Eq. (8)).

3. Materials and methods

3.1. Site description and experimental design

The experimental field is located at Bekkevoort, Belgium. It is situated on a gentle slope and is covered with a meadow. The soil is classified as a Eutric Regosol. Typically, the top 100 cm show three soil horizons: an Ap horizon between 0 and 25 cm, a C1 horizon between 25 and 55 cm and a C2 horizon between 55 and 100 cm (Mallants, 1996). Dye studies revealed the occurrence of macropores throughout the soil profile, mainly from biological origin (Vanderborght et al., 2000). Previous studies characterized the soil hydraulic and solute transport parameters on different scales and under different flow conditions (Mallants et al., 1996; Vanderborght, 1997; Jacques et al., 1997, 1998).

A trench, 1.2 m deep and 12 m long, was dug at the field site. Textural analyses were done at different depths in the trench (Table 1). Next to the trench, the vegetation was removed from the soil surface over an area of 8×2 m^2 and the surface was leveled. An overview of the experimental set-up and the data collected is given in Table 2. One side of the trench was covered using a plastic sheet as a barrier to hydraulically isolate the disturbed trench zone. Along a transect of 5.5 m, two-rod TDR-probes (25 cm long, 0.5 cm rod diameter, 2.5 cm rod spacing) were installed each 50 cm (12 locations) at 5 depths (15, 35, 55, 75, and 95 cm deep). Tension cups (6 mm diameter, 25 mm long) were installed at a horizontal distance of 10 cm from each TDR-probe. Temperature probes (6 cm long) were installed at five depths on three locations at 1.3, 2.7, and 4.2 m from the first

Table 2
Overview of measured variables, used experimental devices, and frequency of measurements (A: automated, M: manual, d: number of depths, p: number of positions)

Quantity	Device	Frequency	Method	Total positions
Water content, θ	TDR-probes	Every 2 h	A	$5d \times 12p$
Resident solute concentration, C^r	TDR-probes	Every 2 h	A	$5d \times 12p$
Pressure head, ψ	Tension cups	Every h	A	$5d \times 12p$
Temperature, T	Temperature probes	Every h	A	$5d \times 3p$
Water fluxes	PCAPS	Every 2/3 d	M	$2d \times 3p$
Solute fluxes	PCAPS	Every 2/3 d	M	$2d \times 3p$
Rainfall	Pluviograph	Continuously	A	1

probe. The travel time of an electromagnetic wave along the lines of the TDR-probe and the reflection coefficient were automatically measured every 2 h using the system described by Heimovaara and de Water (1991). Each probe was calibrated using the techniques of Heimovaara et al. (1995) to obtain the apparent dielectric constant, K_a, and the bulk soil electrical conductivity, EC_a (dS m^{-1}), from the measurements. The water content, θ, was calculated from K_a using a site-specific calibration curve (Jacques et al., 1999). The resident solute concentration was determined from converting EC_a to the electrical conductivity of the soil water, EC_w, by the empirical model of Vogeler et al. (1996) (see Jacques, 2000 for details). Finally, EC_w [dS m^{-1}] was converted to C^r using a linear relationship with a slope of 0.667 and an intercept of -0.52 (Jacques et al., 1998). Pressure heads were automatically recorded using pressure transducers in the set-up of Bertuzzi et al. (1996). Rainfall was continuously measured with a rainfall recorder (200 cm^2) with a floated pen system on a paper (0.1 mm intervals, rotation speed of 1 cm h^{-1}).

After all devices were installed, the trench was refilled and a thin layer of gravel (between 1 and 2 cm) was put on the experimental area to decrease the erosive effect of raindrops on the bare soil surface, minimize evaporation and decrease the weed growth which were regularly removed. Measurements were started on March 11, 1998, defined as day 0. On an area of 16 m^2, 6000 g of a tracer ($CaCl_2{\cdot}2H_2O$) was manually applied on August 28, 1998 (day 168.5) over a period of 3.5 h using a water depth of 0.5 cm with a total concentration of 75 g l^{-1}. The experiment ended on March 31, 1999 (day 384). A throughout discussion of the experimental results and the qualitative interpretation was given in Jacques (2000).

3.2. Overview of measurement sets used in the inverse optimization

We used four different measurement sets in the inverse optimization: $\mathbf{g}_{\theta,d}$, $\mathbf{g}_{\psi,d}$, $\mathbf{g}_q$, and $\mathbf{g}_{c,d}$, where (1) $\mathbf{g}_{\theta,d}$ is a vector containing the water content data averaged by depth for the dth depth ($d = 1$ for the 15 cm depth, $d = 2$ for the 35 cm depth,…, $d = 5$ for the 95 cm depth). Only four daily observations (at 0, 6, 12, and 18 h) were included in the objective function. (2) $\mathbf{g}_{\psi,d}$ is a vector containing the pressure head data averaged by depth for the dth depth and four observations a day. (3) $\mathbf{g}_q$ is a vector containing the hourly rainfall rates that are smaller then 0.5 cm h^{-1}. The decision to include $\mathbf{g}_q$ in Φ was based on preliminary optimizations (results not shown). The upper boundary was defined as hourly rainfall rates as defined above. In preliminary simulations with no surface run-off (thus with surface ponding), a build-up of water of about 10 cm height during some heavy rainfall periods was simulated. However, ponding of water was not observed at the experimental field. On the other hand, only a small part of the precipitation water was actually infiltrating into the soil in simulations with surface run-off (and no $\mathbf{g}_q$ in Φ). The occurrence of excessive run-off was not observed at the field. By including $\mathbf{g}_q$ in Φ, the optimization will search for parameters for which nearly all water infiltrates during moderate rainfall ($q < 0.5$ cm h^{-1}). (4) $\mathbf{g}_{c,d}$ is a vector containing the time-integral-normalized resident concentrations averaged by depth, $C_d^{rt^*}(t)$ [T^{-1}] defined as (Vanderborght et al., 1996; Jacques et al., 1998):

$$C_d^{rt*}(t) = \frac{\theta_d(t)C_d^r(t)}{\int_0^\infty \theta_d(u)C_d^r(u)\mathrm{d}u} \tag{10}$$

where θ_d and C_d^r are the water content and the resident solute concentration averaged by depth, respectively. For the transient flow problem in this study, a sensitivity analysis has shown that the effect of the calibration coefficients for EC_w on $C_d^{rt*}(t)$ is very small and smaller than when $C_d^r(t)$ is used.

3.3. Inverse procedures

Two different approaches were used for the estimation of the water flow and solute transport parameters. In the first approach (Section 4.1), parameters are estimated using time series of observations for a particular depth assuming a homogeneous soil profile. Parameters are interpreted as effective parameters representative for an equivalent homogeneous porous medium between the soil surface and a particular depth. Thus, we seek to minimize, for example, the objective function $\Phi(\mathbf{g}_{\theta,d}, \mathbf{g}_{\psi,d}; \mathbf{b}_{hde})$, i.e. to optimize the effective (subscript e) water flow parameters of the dth depth using time series of the averaged θ and ψ

for the dth depth. In the second approach (Section 4.2), a layered soil profile with different parameters for each layer is assumed. The layers are defined between two observation depths. For example, the objective function $\Phi(\mathbf{g}_{\theta,d}, \mathbf{g}_{\psi,d}, \mathbf{g}_{\theta,d-1}, \mathbf{g}_{\psi,d-1}, \mathbf{g}_{\theta,d-2}, \mathbf{g}_{\psi,d-2}; \mathbf{b}_{\mathrm{h}d} | \mathbf{b}_{\mathrm{h}d-1}, \mathbf{b}_{\mathrm{h}d-2})$ leads to the estimation of the water flow parameters for the layer between the $(d-1)$th and dth depth. The time series of averaged θ and ψ for the $(d-2)$th, $(d-1)$th and dth depth are used in this inversion procedure and parameters of the upper two layers are assumed to be previously estimated.

In both approaches, parameters are estimated in two steps. In approach 1, $\mathbf{b}_{\mathrm{h}de}$ is first estimated using $\mathbf{g}_{\theta,d}$, $\mathbf{g}_{\psi,d}$ and $\mathbf{g}_q$, followed by the estimation of the solute transport parameters ($\mathbf{b}_{\mathrm{se}}$ or $\mathbf{b}_{\mathrm{sne}}$) using $\mathbf{g}_{c,d}$ and $\mathbf{b}_{\mathrm{h}de}$. A similar sequential approach is used in the second approach in which the different layers are subsequently added to a soil profile of 150 cm deep from the top to the bottom layer. Parameters for particular layers, $\mathbf{b}_{\mathrm{h}d}$ are estimated in a sequence starting from the top layer. When all sets of $\mathbf{b}_{\mathrm{h},d}$ are estimated, some further tuning is done by re-estimating combinations of $\mathbf{b}_{\mathrm{h},d}$ from different layers. When all hydraulic parameters are estimated, the same stepwise procedure is used to estimate the solute transport parameters.

Although Mishra and Parker (1989) recommended to simultaneously estimate the soil hydraulic and solute transport parameters (see Inoue et al., 2000), we used the sequential approach to minimize problems of non-uniqueness, especially for approach 2 having up to 36 unknown parameters. To test uniqueness of the optimized parameters, $\Phi(\mathbf{g}_{\theta,d}, \mathbf{g}_{\psi,d}; \mathbf{b}_{\mathrm{h}de})$ for $d = 1$, 2, and 3 were minimized for different initial parameter sets. Final estimates were close to each other and their 95% confidence interval overlapped (results not shown). Since solute transport is influenced by water flow and thus by the soil hydraulic properties (Medina and Carrera, 1996), hydraulic and solute transport parameters were also optimized simultaneously by minimizing $\Phi(\mathbf{g}_{\theta,d}, \mathbf{g}_{\psi,d}, \mathbf{g}_{c,d}; \mathbf{b}_{\mathrm{h}de}, \mathbf{b}_{sede})$ with $d = 2$ and 3 using the previously optimized parameters from the sequential approach as initial parameters. No significant differences in parameter estimates were found between the simultaneous and sequential approach (results not shown). Based on these findings, we used the sequential approach and only one initial parameter set for all optimization problems.

4. Results

4.1. Approach 1: equivalent homogeneous soil profile

First, we discuss the effective hydraulic parameters estimated by minimizing $\Phi(\mathbf{g}_{\theta,d}, \mathbf{g}_{\psi,d}, \mathbf{g}_q; \mathbf{b}_{\mathrm{h}de})$. Results are shown in Figs. 1–4 and Tables 3–5. Since water contents and pressure heads in the fifth depth showed little temporal variability, we used the time series of

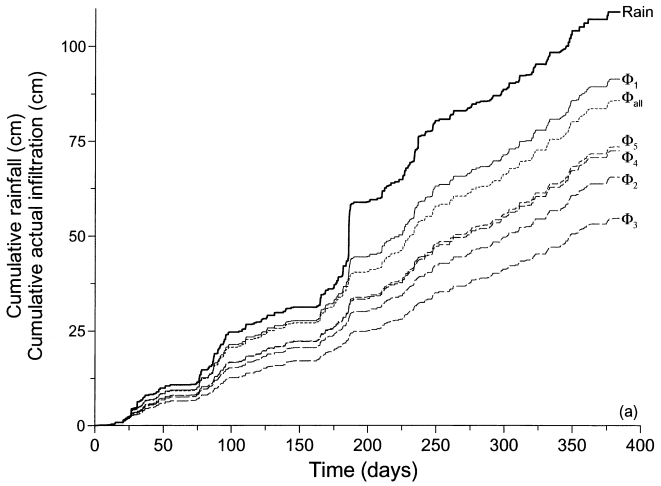

Fig. 1. Measured cumulative rainfall and simulated cumulative actual infiltration for the different objective functions as defined in Table 3.

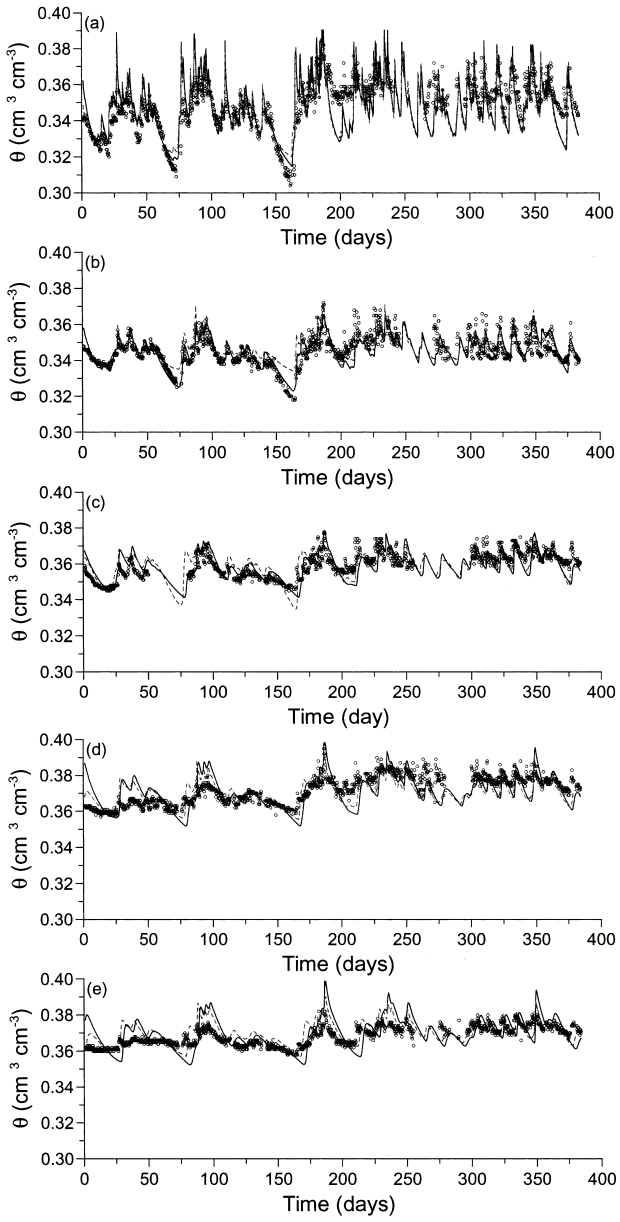

Fig. 2. Measured water contents, and water contents simulated using the equivalent homogeneous approach (approach 1, solid line), and multi-layered soil approach (approach 2, Φ_{all} in Table 3, dashed line) for (a) 15 (Φ_1 in Table 3 for approach 1), (b) 35 (Φ_2 in Table 3 for approach 1), (c) 55 (Φ_3 in Table 3 for approach 1), (d) 75 (Φ_4 in Table 3 for approach 1), and (e) 95 (Φ_5 in Table 3 for approach 1) cm depth.

the fourth and fifth depth simultaneously to estimate the parameters for the fifth depth (Table 3). There is only a small difference between the parameters of the different depths. A detailed discussion of the optimized parameters will be given in Section 4.2.

For the five optimizations, the total simulated cumulative infiltration is only between 50.2 and 83.8% of the total amount of rain (Table 3). Fig. 1 shows that the largest difference occurred during the heavy rainfall on day 185, and smaller differences

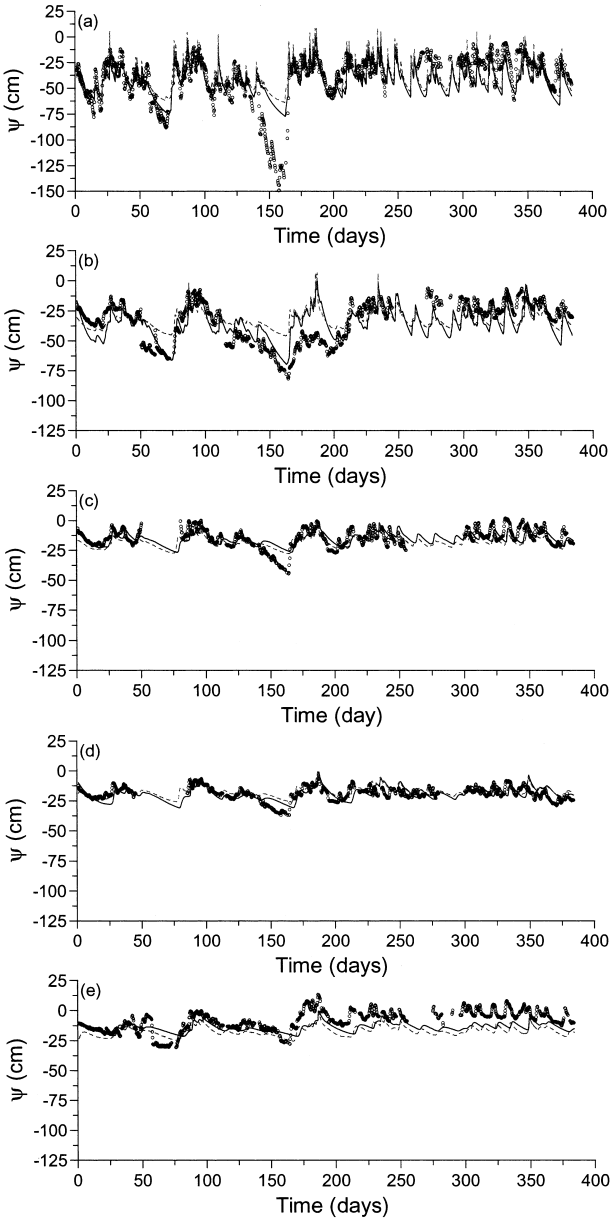

Fig. 3. Measured pressure heads, and pressure heads simulated using the equivalent homogeneous approach (approach 1, solid line), and multi-layered soil approach (approach 2, Φ_{all} in Table 3, dashed line) for (a) 15 (Φ_1 in Table 3 for approach 1), (b) 35 (Φ_2 in Table 3 for approach 1), (c) 55 (Φ_3 in Table 3 for approach 1), (d) 75 (Φ_4 in Table 3 for approach 1), and (e) 95 (Φ_5 in Table 3 for approach 1) cm depth.

during moderate rainfall conditions (e.g. between days 100 and 150, and 250 and 350, except for $\Phi(\mathbf{g}_{\theta,1}, \mathbf{g}_{\psi,1}\mathbf{g}_q; \mathbf{b}_{\mathrm{h1e}})$). These differences may be due to either surface run-off across the slope, either infiltration in the soil in macropores, or a combination of both. It was not possible to discriminate between both processes because run-off was not measured (although no large run-off flow was observed during the experiment), and measurements of water content and pressure head generally do not indicate preferential

flow. However, macropore infiltration might be an important process. During the same experiment, water and solute fluxes were measured at two depths and three locations with passive capillary wick samplers. Qualitative interpretation of these measurements indicated the occurrence of significant macropore water flow as was discussed in Jacques (2000). The dynamics of water content and pressure head time series gradually decreased with depth, but the effect of heavy rainfalls was still clearly observed at deeper depths by a sudden increase in θ after heavy rain events. A low conductivity is needed to model the slow water flow dynamics at deeper depths, whereas a high conductivity is required to model the fast responses after heavy rainstorms. The model has solved this dilemma by generating a large amount of run-off, even during moderate rainfall conditions.

Simulations very well reproduced the dynamics of the water content with time, especially between days 80 and 140 and during the last 100 days of the experiment (Fig. 2). At the fourth and fifth depths, the calculated water contents overpredicted the dynamics of the observed water contents, especially between days 25 and 150. Furthermore, the dynamics of the calculated water contents are somewhat retarded compared with the observations during the last 150 d of the experiment. Visual inspection of Fig. 3 shows that pressure head simulations are less good than the ones for the water content. However, pressure heads that were measured in smaller soil volumes may be associated with larger uncertainties than water contents that are measured in larger soil volumes using TDR-probes. In addition, external factors such as variation in temperature and the long capillary tubes between suction cup and pressure transducer may result in larger uncertainties of the pressure head measurements. Calculated pressure heads decreased less compared to observations during the dry period in the summer (day 140–160). Although a thin layer of gravel was put on the soil surface, some water loss due to evaporation may have caused this discrepancy between measurements and observations. Note that the difference between measured and simulated water contents during this period was less pronounced. At the second depth, pressure heads are significantly overpredicted between days 150 and 200. This may be rather due to measurement errors and uncertainty than due to an incorrect model. Water contents during this period were as large as around day 100 or during the last 100 d of the experiment. However, during these periods, the pressure heads were larger than between days 150 and 200.

Subsequently, the transport parameters were determined using the solute breakthrough data. We will first discuss the results for the CDE- and MIM-models for the second to fifth depth (Fig. 4(b)–(e)). For the second, third and fourth depths, the MIM-model describes the observed breakthrough curves better than the CDE-model, especially in the tailing part. In contrast to the simulations presented here, one usually expects that the tailing of the MIM-model will be more pronounced than that of the CDE-model. The optimization algorithm may have resulted in an overestimation of the dispersivity values for the CDE-model in order to describe the fast breakthrough. Consequently, the tailing of the breakthrough curve is also overestimated. At the fifth depth, the MIM-model simulated better the early breakthrough but overpredicted the tailing compared to the CDE-model.

Fitted effective solute transport parameters are given in Table 5. Dispersivity values increase significantly with depth, which was also observed for steady-state lysimeter (Vanderborght et al., 2000) and in situ (Jacques et al., 1998), and transient lysimeter (Vanderborght et al., 2000) solute transport experiments on the same soil. Immobile water contents were high at the second and fifth depth compared to small values at the other two depths. Extremely low ω values were obtained for these two depths compared to values reported in the literature (see compiled values in Vanderborght et al., 1997).

We could not describe the solute breakthrough curve at the first depth using the CDE or the MIM-model. The 'best' fit of the MIM-model showed a very large peak just after solute application (with a maximum C^{rt*} of 0.195) followed by an extreme long tailing (with $\lambda = 643$ cm, $\Phi(\mathbf{g}_{C,1}; \mathbf{b}_{\mathrm{sne1e}} | \mathbf{b}_{\mathrm{h1e}}) = 0.821$, results not shown). A major reason for this failure may be the difference between the actual infiltration processes at the soil surface during solute application and the processes described in the MIM-model. The soil consists of different flow domains that can be subdivided into two groups: (i) preferential flow paths, mainly macropores in this soil, and (ii) the soil matrix consisting of domains of slowly moving water and immobile water (see Jacques, 2000). In our

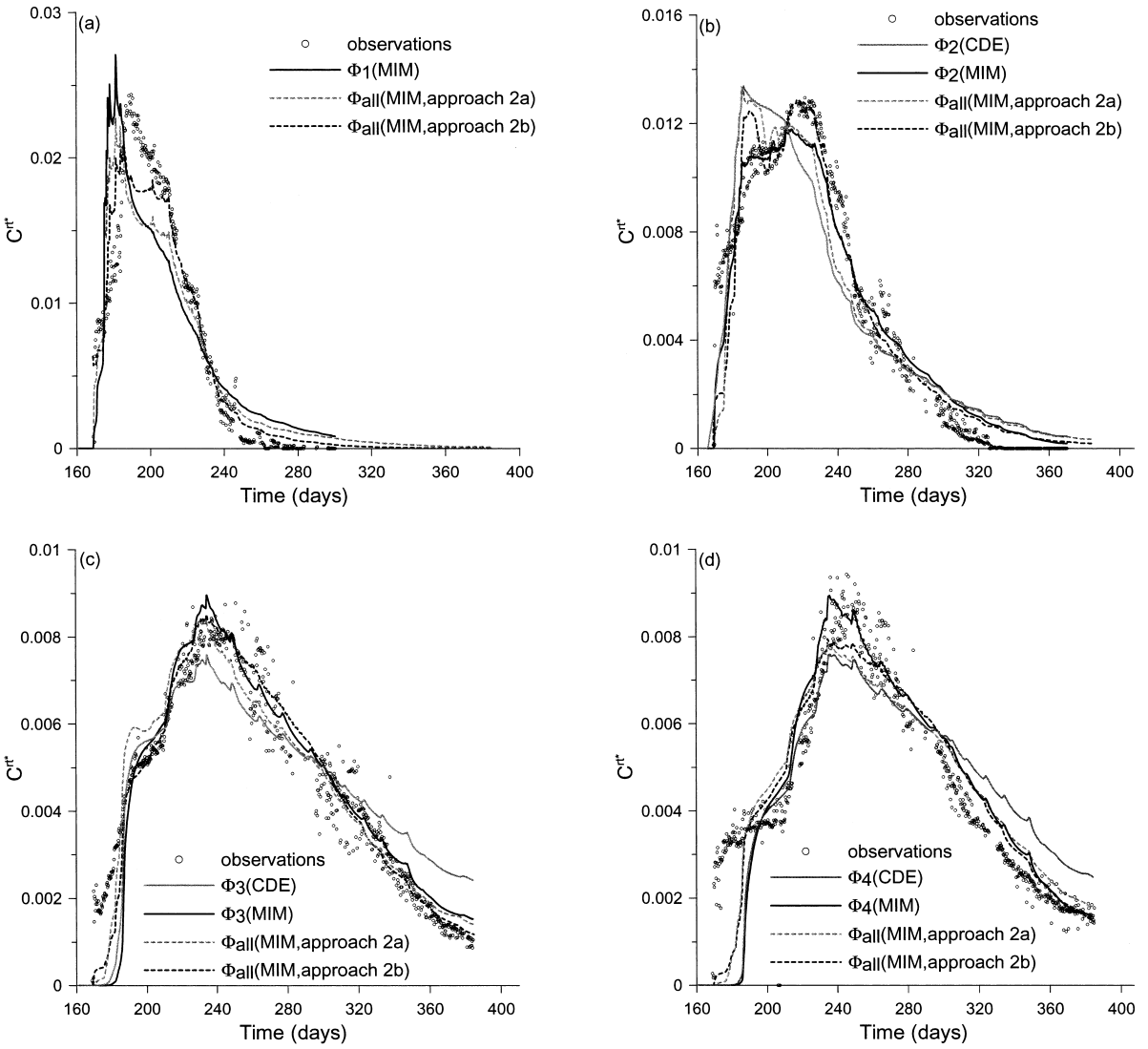

Fig. 4. Time-integral-normalized resident concentrations measured and simulated for (a) 15, (b) 35, (c) 55, (d) 75, and (e) 95 cm depth for the objective functions as defined in Table 5.

field experiment, solutes were applied after a long dry period, and it is reasonable to assume that water entered both the soil matrix due to sorptivity effects and in the preferential flow domain consisting mainly of macropores (water may flow into macropores under no ponding conditions as shown by Godrathi et al. (1999)). Water in the preferential flow domain reached the 15 cm depth immediately after solute application. A second peak in the breakthrough curve indicated the solute arrival in the slowly flowing water in the soil matrix, while tailing may indicate diffusive solute exchange between mobile and immobile water (Jacques, 2000). All solute applied at the soil surface will move only into the mobile water phase for the MIM-model. Only a small amount of solute will be exchanged to the immobile water content since the transport distance is small and the exchange time short. A dual- or multi-porosity transport model (e.g. Jarvis et al., 1991; Gerke and van Genuchten, 1993; Steenhuis et al., 1990; Skopp and

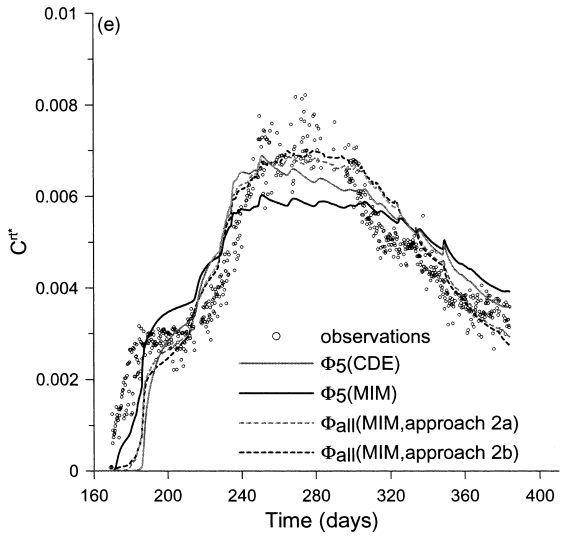

Fig. 4. (*continued*)

Gardner, 1992) may be more appropriate to represent the transport processes near the soil surface.

Alternatively, a mixing zone near the soil surface, in which solutes are distributed over the different flow regions, may mimic these processes. We defined a 5 cm thick layer at the soil surface with similar hydraulic properties as the rest of the soil profile, but with only mobile water (i.e. CDE). The dispersivity of this first mixing layer and parameters of the MIM-model for the other layer were estimated using the observed breakthrough data at the 15 cm depth. A value of 2.2 was obtained for λ of the mixing layer (see Table 5 for other parameters). Although the value of the objective function for the two-layered system of the first depth is the largest, an acceptable description of the observed breakthrough curve is obtained (Fig. 4(a)) given the complex transport mechanisms near the soil surface.

In conclusion for the estimated effective parameters: (i) time series of water contents, pressure heads and resident solute concentrations are reasonably well described, (ii) the MIM-model described the peak and tailing parts of the observed solute breakthrough curves better than the CDE-model, and (iii) goodness-of-fit of the BTCs showed a decreasing trend with depth (except for the breakthrough curve at the first depth).

4.2. Approach 2: multi-layered soil profile

Based on the results of the first approach, four layers for hydraulic properties (fourth and fifth

Table 3
Summary of statistical measures of goodness-of-fit for time series of water contents, pressure heads and precipitation rates (MSE—mean squared error). Φ is the objective function as defined in Eq. (8) for the three measurement sets (water content, pressure head, and rainfall rates). Φ_θ, Φ_ψ, and Φ_q are the objective functions as defined in Eq. (8) using only one measurement set ($j = 1$), (i.e. water content, pressure head, and rainfall rates, respectively) calculated for the parameters obtained by minimizing Φ

	Φ	Φ_θ	Φ_ψ	Φ_q	R^2	%TF[a]	MSE_θ ($\times 10^{-5}$)	MSE_ψ
Approach 1: equivalent homogeneous soil profile								
$\Phi(\mathbf{g}_{\theta,1}, \mathbf{g}_{\psi,1}, \mathbf{g}_q; \mathbf{b}_{h1e}) = \Phi_1$	1.287	0.656	0.542	0.089	0.86	83.8	12.5	317.9
$\Phi(\mathbf{g}_{\theta,2}, \mathbf{g}_{\psi,2}, \mathbf{g}_q; \mathbf{b}_{h2e}) = \Phi_2$	1.984	0.607	0.717	0.66	0.854	60.1	4.1	205.7
$\Phi(\mathbf{g}_{\theta,3}, \mathbf{g}_{\psi,3}, \mathbf{g}_q; \mathbf{b}_{h3e}) = \Phi_3$	2.415	0.812	0.725	0.877	0.813	50.2	3.98	45.4
$\Phi(\mathbf{g}_{\theta,4}, \mathbf{g}_{\psi,4}, \mathbf{g}_q; \mathbf{b}_{h4e}) = \Phi_4$	2.543	1.05	0.992	0.5	0.913	66.4	6.21	31.1
$\Phi(\mathbf{g}_{\theta,4}, \mathbf{g}_{\psi,4}, \mathbf{g}_{\theta,5}, \mathbf{g}_{\psi,5}, \mathbf{g}_q; \mathbf{b}_{h5e}) = \Phi_5$	2.925	1.385	1.073	0.467	0.748	67.4	3.79	79.2
Approach 2: layered soil profile								
$\Phi(\text{all})^b = \Phi_{all}$						78.6		
15 cm depth							11.6	350.6
35 cm depth							3.85	243.3
55 cm depth							4.1	42.4
75 cm depth							4.21	27.9
95 cm depth							3.46	120.1

[a] The ratio of the total simulated cumulative flux at the top boundary over the cumulative amount of rain (109 cm) multiplied by 100.
[b] The total objective function of the second approach includes all three-time series. All hydraulic parameters are estimated simultaneously.

Table 4
Estimated hydraulic parameters based on time series of water contents, pressure heads and precipitation rates

	θ_s	α (cm^{-1})	n	K_s ($cm\ d^{-1}$)	l
Approach 1: equivalent homogeneous soil profile					
$\Phi(\mathbf{g}_{\theta,1}, \mathbf{g}_{\psi,1}, \mathbf{g}_q; \mathbf{b}_{h1e})$	0.390	0.0173	1.43	5.18	4.70
$\Phi(\mathbf{g}_{\theta,2}, \mathbf{g}_{\psi,2}, \mathbf{g}_q; \mathbf{b}_{h2e})$	0.369	0.0137	1.38	1.64	0.13
$\Phi(\mathbf{g}_{\theta,3}, \mathbf{g}_{\psi,3}, \mathbf{g}_q; \mathbf{b}_{h3e})$	0.378	0.0251	1.41	1.31	5.62
$\Phi(\mathbf{g}_{\theta,4}, \mathbf{g}_{\psi,4}, \mathbf{g}_q; \mathbf{b}_{h4e})$	0.399	0.0248	1.435	2.31	5.25
$\Phi(\mathbf{g}_{\theta,4}, \mathbf{g}_{\psi,4}, \mathbf{g}_{\theta,5}, \mathbf{g}_{\psi,5}, \mathbf{g}_q; \mathbf{b}_{h5e})$	0.399	0.0355	1.435	2.55	5.25
Approach 2: multi-layered soil profile					
Φ(all)[a]					
15 cm depth	0.378	0.0137	1.56	3.89	0.395
35 cm depth	0.371	0.0137	1.55	1.55	0.12
55 cm depth	0.37	0.0246	3.35	1.22	0.001
75 + 95 cm depth	0.391	0.0219	1.57	2.35	15.28

[a] The total objective function of the second approach includes all three-time series. All hydraulic parameters are estimated simultaneously.

depth were combined in one layer) and five layers for transport properties were defined. In addition, we did not use the CDE-model, and defined a 5 cm thick mixing layer containing only mobile water near the soil surface. Thus, 20 soil hydraulic and 16 solute transport parameters were estimated (approach 2a). Alternatively, the mixing layer was defined as an initial value problem (approach 2b). Solutes were evenly distributed over the immobile and mobile water content to a depth of 1.44 cm (= 0.5 cm applied water divided by the average water content in that depth interval, 0.347 $cm^3\ cm^{-3}$) and only 15 transport parameters were estimated. Results are summarized in Tables 3–5 and Figs. 1–4.

The total actual infiltration at the soil surface is close to the value obtained by minimizing $\Phi(\mathbf{g}_{\theta,1}, \mathbf{g}_{\psi,1}, \mathbf{g}_q; \mathbf{b}_{h1e})$ and is 85.7 cm. This value is substantially larger than the total actual infiltration obtained for the other four objective functions used for estimating effective parameters for deeper depths. As discussed above, in order to represent the decrease in the water flow dynamics with depth in the equivalent homogeneous approach, a large part of the rainfall did not infiltrate in the soil. The multi-layered soil profile had a dampening effect on the water flow reducing the dynamics deeper in the soil.

Visual inspection of Figs. 2 and 3 shows that approach 1 described the observed time series somewhat better than approach 2 (see also MSE in Table 3). There are only small differences between the two approaches in terms of the MSE. MSE_ψ are larger for the first, second and the last depth for approach 2 compared to approach 1. Except for the third depth, approach 2 performed somewhat better than approach 1 for water contents based on MSE_θ.

A quantitative comparison between the three methods to estimate the MIM-model parameters (approach 1, 2a, and 2b) is based on the MSE for the five individual observation depths (Table 5). The results from approach 1 are worse than those obtained for approaches 2a and 2b. Approach 2b performed better at all depths compared to approach 2a. However, the difference between the 2a and 2b decreased with depth: the MSE of 2b is 38.5, 55.1, 77.1, 82.7, and 98.6% of that of 2a. The two approaches used to mimic the complex flow patterns in the topsoil have the largest impact on the simulations of solute breakthrough in the upper horizons with an obvious preference for approach 2b.

However, the better simulation results obtained with approach 2 are not consistent with depth, as can be seen in Fig. 4. For example, approach 2b obviously resulted in a better description of the tailing part of the breakthrough curve at the first depth or of the solute peak between days 220 and 240 for the second depth. On the other hand, approach 2a and 2b failed to describe C^{rt*} between days 185 and 210 in contrast to approach 1 (MIM-model). At the other three depths, there are only small differences between approaches 2a and 2b, although 2b described the measured concentrations between days 185 and 210 somewhat better, especially at the third depth.

Table 5
Summary of statistical measures of goodness-of-fit and estimated solute transport parameters for time series of resident solute concentrations (MSE—mean squared error, na—not available)

	Φ	R^2	MSE_C ($\times 10^{-6}$)	λ (cm)	θ_{im} ($cm^3\ cm^{-3}$)	ω (d^{-1})
Approach 1: equivalent homogeneous soil profile						
CDE-model						
$\Phi(\mathbf{g}_{C,1};\mathbf{b}_{se1e}\|\mathbf{b}_{h1e}) = \Phi_1$(CDE)	na	na	na	na	–	–
$\Phi(\mathbf{g}_{C,2};\mathbf{b}_{se2e}\|\mathbf{b}_{h2e}) = \Phi_2$(CDE)	0.146	0.854	3.22	8.45	–	–
$\Phi(\mathbf{g}_{C,3};\mathbf{b}_{se3e}\|\mathbf{b}_{h3e}) = \Phi_3$(CDE)	0.215	0.785	1.11	19.96	–	–
$\Phi(\mathbf{g}_{C,4};\mathbf{b}_{se4e}\|\mathbf{b}_{h4e}) = \Phi_4$(CDE)	0.376	0.648	1.83	15.84	–	–
$\Phi(\mathbf{g}_{C,5};\mathbf{b}_{se5e}\|\mathbf{b}_{h5e}) = \Phi_5$(CDE)	0.314	0.794	0.84	21.72	–	–
MIM-model						
$\Phi(\mathbf{g}_{C,1};\mathbf{b}_{sne1e}\|\mathbf{b}_{h1e})$[a]$= \Phi_1$(MIM)	0.306	0.697	19.7	3.227	0.32	0.019
$\Phi(\mathbf{g}_{C,2};\mathbf{b}_{sne2e}\|\mathbf{b}_{h2e}) = \Phi_2$(MIM)	0.05	0.958	1.1	1.98	0.32	0.059
$\Phi(\mathbf{g}_{C,3};\mathbf{b}_{sne3e}\|\mathbf{b}_{h3e}) = \Phi_3$(MIM)	0.158	0.878	0.82	11.05	0.053	$3.0\ 10^{-7}$
$\Phi(\mathbf{g}_{C,3};\mathbf{b}_{sne3e}\|\mathbf{b}_{h3e}) = \Phi_3$(MIM)	0.279	0.806	1.35	10.6	0.048	$4.7\ 10^{-7}$
$\Phi(\mathbf{g}_{C,4};\mathbf{b}_{sne4e}\|\mathbf{b}_{h4e}) = \Phi_4$(MIM)	0.260	0.755	0.69	22.65	0.325	0.038
Approach 2: multi-layered soil profile						
MIM-model; approach 2a						
$\Phi(\cdot) = \Phi_{all}$(MIM, approach 2a)	0.1514	0.849				
15 cm depth			12.1	0.067	0.32	0.05
35 cm depth			3.01	8.74	0.32	0.089
55 cm depth			0.51	7.65	0.32	0.045
75 cm depth			1.22	53.9	0.32	0.028
95 cm depth			0.64	3.28	0.32	0.027
MIM-model: approach 2b						
$\Phi(\cdot) = \Phi_{all}$(MIM, approach 2b)	0.078	0.922				
15 cm depth			4.66	0.433	0.327	0.12
35 cm depth			1.66	5.66	0.322	0.086
55 cm depth			0.39	6.88	0.3033	0.027
75 cm depth			1.01	35.45	0.32	0.027
95 cm depth			0.62	2.99	0.32	0.02

[a] Estimated with a 5 cm thick surface layer consisting of only mobile water (i.e. CDE).

Compared to approach 1, approaches 2a and 2b predicted earlier breakthrough, although there is still a significant difference with the observed early breakthrough. The tailing part is well described by all methods using the MIM-model. The opposite is observed for the fifth depth: approach 1 described better the early breakthrough, whereas the approaches 2a and 2b fitted better the peak and tailing of the breakthrough.

4.3. Comparison of estimated parameters with previous parameter values

The α-coefficient of Eqs. (2) and (3) showed an increasing trend with depth, while n is constant with depth, except at the 55 cm depth for the layered soil profile (Table 4). At that depth, the high n value is somewhat compensated by the low l-parameter. The estimated values, reported in Table 4, are compared with parameter values determined in earlier studies on the same soil (Table 6). The equilibrium desorption $\theta - \psi$ measurements resulted in smaller α-values and similar n-values. The contrary was observed for the transient drainage experiment: similar α-values (except between 5 and 15 cm), but smaller n-values. Furthermore, α and n parameter values were different for $K(\psi)$ based on the drainage experiment. The results of Mallants et al. (1997a) indicate using the same parameters in Eqs. (2) and (3) may be too restrictive for modeling transient water flow in soils.

Table 6
Overview of parameters of the water retention characteristic and the unsaturated hydraulic conductivity described with Eqs. (2) and (3), respectively, determined in previous experiments on the same soil (upper and lower positions refers to depths in the profile for which parameters were estimated)

	Experimental information					Parameter values				Reference
	Method	Diameter (cm)	Height (cm)	Upper position (cm)	Lower position (cm)	Parameter	Mean	Minimum	Maximum	
$\theta(\psi)$	Desorption technique	5	5	10	90	α		0.0038	0.013	Mallants et al., 1997a
						n		1.311	1.535	Mallants et al., 1997a
	Transient drainage experiment	30	100	5	15	α		0.103	0.147	Mallants et al., 1997a
				30	60	α		0.017	0.031	Mallants et al., 1997a
				5	90	n		1.05	1.14	Mallants et al., 1997a
$K(\psi)$	Instantaneous profile method	30	100	0	–	α		0.038	0.065	Mallants et al., 1997a
						n		2.63	2.85	Mallants et al., 1997a
	Constant head method	5	5	10	90	K_s	333.6			Mallants et al., 1997b
		20	20	0	–	K_s	126.7			Mallants et al., 1997b
		30	100	0	–	K_s	11.8	0.96	12.7	Mallants et al., 1997b

The K_s-values measured on the lysimeters of 100 cm height are comparable with the fitted ones from our field data. Note the different boundary conditions used to estimate K_s: a laboratory method with ponding conditions for the former in contrast to an in situ method with natural boundary for the latter.

The estimated immobile water content for approach 2 is high in each layer (Table 5). Vanderborght et al. (2000) also found small mobile water contents in their transient flow experiments on the same soil. In contrast to our study, they noticed a decrease in θ_m with depth. For approach 2b, transfer coefficients, ω, show a decreasing trend with depth and are in the same order as values reported for the same soil for steady-state saturated solute transport (0.0384–0.744 d^{-1}, Mallants et al., 1996). These are smaller than the value (0.89 d^{-1}) obtained for the transient flow experiments of Vanderborght et al. (2000). The dispersivity of the fourth depth is large compared to values derived for the other depths. This is probably due to an artifact, since the optimization algorithm, based on minimizing the sum of squared errors, tried to describe both the fast breakthrough and the long tailing of the observed breakthrough curve. The small dispersivity value of the fifth depth is due to a combination of the high dispersivity value of the fourth depth and the incomplete measurement of the tailing part of the breakthrough curve.

5. Final comments and conclusions

Although modeling based on inverse optimization could describe some of the main features of the experimental data, and although estimated parameters are within the range of earlier determined flow and transport parameters, this study also shown that the combination of Richards' equation and the MIM-model failed to describe important features such as 'internal run-off' and early solute breakthrough under natural flow conditions in a structured soil. Some model improvements are proposed here, which are to be considered in further studies. A unimodal description (e.g. Eqs. (2) and (3)) of the hydraulic characteristics may not describe the fast increase in hydraulic conductivity near saturation when macropores or structural elements are present in the soil. When a medium with multiple flow domains (e.g. matrix and macropores) is represented by an equivalent continuum (van Genuchten et al., 1999), the hydraulic characteristics can be described by multi-modal functions (e.g. Durner, 1994; Mohanty et al., 1997, 1998). The hydraulic conductivity then increases drastically near saturation without a large increase in pressure head or water content resulting in a larger amount of actual infiltration under wet condition or during heavy rainfall as observed in our study.

Transient flow processes may significantly

complicate the parametric description of the solute transport processes and result in flow-dependency of solute transport parameters. Vanderborght et al. (2001) compiled the solute transport parameters for different tracer experiments in key Belgian soil types. They found that longitudinal dispersivity increased with increasing water flux J_w, implying that dispersivity cannot be viewed entirely as a material constant, but is also dependent on the flow conditions. For the soil type used in this study, Vanderborght et al. (2000) found that for conditions close to saturation this relation is $\lambda = 3.44 J_w^{0.83}$. Based on the relations between dispersivity, depth and flow rates at one hand and the length of the pores at the other hand (Skopp and Gardner, 1992), Vanderborght et al. (2000) concluded that long continuous pores were activated when flow rates increased. The experimental studies of Reedy et al. (1996) and Bajracharya and Barry (1997) indicated that ω may also increase with flow velocity. A modeling study of Zurmühl and Durner (1996) showed that treating θ_{im} as an dynamic variable may significantly influence the simulation of solute transport through structured soils.

The MIM-model did not represent the complex flow and transport mechanisms, especially near the soil surface (Fig. 4). Snow et al. (1994) also observed that solute transport near the soil surface was different from transport processes deeper in the soil. They stated that applied solutes move quickly into the immobile water and then slowly diffuse back to the mobile water. This process was mimicked here by approach 2b. An alternative is to use dual-porosity models assuming advective transport in both flow domains (e.g. Jarvis et al., 1991; Gerke and van Genuchten, 1993). A second problem is that the MIM-model assumes that solutes are uniformly distributed in each water phase. As was experimentally demonstrated by Ghodrati et al. (1999), only a small part of the matrix domain interacts with the preferential flow domain, also called the active matrix layer (Wallach and Steenhuis, 1998). Furthermore, lateral mixing processes between different flow domains change with depth (Flühler et al., 1996; Flury et al., 1994; de Rooij, 1996). Multi-region transport models (e.g. Hutson and Wagenet, 1995) may be needed to describe the complex lateral mixing processes between macropores, active matrix layer, and mobile and immobile regions.

As a general conclusion, observed time series of water content, pressure head and solute concentration could reasonable be described by applying the Richards' equation for water flow and the non-equilibrium convection–disperison equation for solute transport given a layered soil profile and defining a kind of mixing layer for solute near the soil surface. We applied successfully the sequential parameter estimation approach to estimate the large number of hydraulic and solute transport parameters needed to describe the field-scale water flow and solute transport under transient flow conditions. However, the applied models failed to describe some specific features such as macropore water flow (failure of Richards' equation) and mixing of solutes between different flow domains (failure of the convection–dispersion equation).

Acknowledgements

This study was done with financial support of a Research Grant of the Fund for Scientific Research-Flanders (Belgium) (F.W.O.- Vlaanderen). The first author acknowledges the financial support of a scholarship of the Flemish Institute for the Encouragement of Scientific–Technological Research in the Industry (IWT). The inverse optimization was performed at the US Salinity Laboratory, USDA-ARS, made possible through a travel grant of the Fund for Scientific Research—Flanders (Belgium) (F.W.O.-Vlaanderen) and a grant of the National Science Foundation—USA. We acknowledge the family Deckers, owners of the experimental field, for the permission to perform these experiments on their property. The assistance of J. Schaerlaekens, F. Serneels, and J. Vanderborght in the field and the laboratory is highly appreciated. The comments of the anonymous reviewer to improve the overall quality of the paper are also highly appreciated.

References

Abbaspour, K., Sonnleitner, M., Schulin, R., 1999. Uncertainty in estimation of soil hydraulic parameter by inverse modeling: example lysimeter experiments. Soil Sci. Soc. Am. J. 63, 501–509.

Abbaspour, K., Kasteel, R., Schulin, R., 2000. Inverse parameter estimation in a layered unsaturated field soil. Soil Sci. 165, 109–123.

Bajracharya, K., Barry, D.A., 1997. Nonequilibrium solute transport parameters and their physical significance: numerical and experimental results. J. Cont. Hydrol. 24, 185–204.

Bertuzzi, P., Gauda, J.C., Bourlet, M., Mohrath, D., Chanzy, A., 1996. Methode de Wind: Notice Technique. Institute National de Recherche Agronomique, Unité du Sol d'Avignon, France, 54 pp.

Butters, G.L., Jury, W.A., 1989. Field scale transport of bromide in an unsaturated soil, 2. Dispersion modeling. Water Resour. Res. 25, 1583–1589.

Carsel, R.F., Parrish, R.S., 1988. Developing joint probability distributions of soil water retention characteristics. Water Resour. Res. 24, 755–769.

de Rooij, G.H., 1996. Preferential flow in water-repellent sandy soils: model development and lysimeter experiments. PhD Dissertation, University of Wageningen, The Netherlands, 229 pp.

Durner, W., 1994. Hydraulic conductivity estimation for soils with heterogeneous pore structure. Water Resour. Res. 30, 211–223.

Flühler, H., Durner, W., Flury, M., 1996. Lateral solute mixing processes—a key for understanding field-scale transport of water and solutes. Geoderma 70, 165–183.

Flury, M., 1993. Transport of bromide and chloride in a sandy and a loamy field soil. PhD Dissertation ETH, NO. 10185, 136 pp.

Flury, M., Flühler, H., Jury, W.A., Leuenberger, J., 1994. Susceptibility of soils to preferential flow of water: a field study. Water Resour. Res. 30, 1945–1954.

Gerke, H.H., van Genuchten, M.Th., 1993. A dual-porosity model for simulating the preferential movement of water and solutes in structured porous media. Water Resour. Res. 29, 305–319.

Ghodrati, M., Chendorain, M., Chang, Y., 1999. Characterization of macropore flow mechanisms in soil by means of a split macropore column. Soil Sci. Soc. Am. J. 63, 1093–1101.

Heimovaara, T., de Water, E., 1991. A computer controlled TDR system for measuring water content and bulk electrical conductivity of soils. Laboratory of Physical Geography and Soil Science, University of Amsterdam, Report no. 41, 27 pp.

Heimovaara, T., Focke, A.C., Bouten, W., Verstraten, J.M., 1995. Assessing temporal variations in soil water composition with time domain reflectometry. Soil Sci. Soc. Am. J. 59, 689–698.

Hutson, J.L., Wagenet, R.J., 1995. A multiregion model describing water flow and solute transport in heterogeneous soils. Soil Sci. Soc. Am. J. 1995, 743–751.

Inoue, M., Šimůnek, J., Shiozawa, S., Hopmans, J.W., 2000. Simultaneous estimations of soil hydraulic and solute transport parameters from transient infiltration experiments. Adv. Water Resour. 23, 677–688.

Jacobsen, O.H., Leij, F.J., van Genuchten, M.Th., 1992. Parameter determination for chloride and tritium transport in undisturbed lysimeters during steady flow. Nordic Hydrol. 23, 89–104.

Jacques, D., 2000. Analysis of water flow and solute transport at the field-scale. PhD, no 454, Faculteit Land bouwkundige en Toegepaste Biologische Wetenschappen, K.U. Leuven, Belgium, 255 pp.

Jacques, D., Vanderborght, J., Mallants, D., Kim, D.-J., Vereecken, H., Feyen, J., 1997. Comparison of three stream tube models predicting field-scale solute transport. Hydrol. Earth Syst. Sci. 4, 873–893.

Jacques, D., Kim, D.-J., Diels, J., Vanderborght, J., Vereecken, H., Feyen, J., 1998. Analysis of steady-state chloride transport through two heterogeneous field soils. Water Resour. Res. 34, 2539–2550.

Jacques, D., Timmerman, A., Feyen, J., 1999. Experimental study of water flow and solute transport in a macroporous soil under natural boundary conditions: Bekkevoort-site description, experimental layout and calibration procedures. Institute for Land and Water Management, K.U. Leuven, Internal Report No. 56, 99 pp.

Jarvis, N., Jansson, P.-E., Dik, P., Messing, I., 1991. Modelling water and solute transport in macroporous soil. I. Model description and sensitivity analysis. J. Soil Sci. 42, 305–319.

Kasteel, R., 1997. Solute transport in an unsaturated field soil: describing heterogeneous flow fields using spatial distribution of hydraulic properties. Dissertation ETH. No. 12,477, 108p.

Lehmann, F., Ackerer, P., 1997. Determining soil hydraulic properties by inverse method in one-dimensional unsaturated flow. J. Environ. Qual. 26, 76–81.

Mallants, D., 1996. Water flow and solute transport in a heterogeneous soil profile. PhD, no 309, Faculteit Landbouwkundige en Toegepaste Biologische Wetenschappen, K.U. Leuven, Belgium, 312 pp.

Mallants, D., Vanclooster, M., Feyen, J., 1996. Transect study on solute transport in a macroporous soil. Hydrol. Proc. 10, 55–70.

Mallants, D., Jacques, D., Tseng, P.-H., van Genuchten, M.Th., Feyen, J., 1997a. Comparison of three hydraulic property measurement methods. J. Hydrol. 199, 295–318.

Mallants, D., Mohanty, B.P., Vervoort, A., Feyen, J., 1997b. Spatial analysis of saturated hydraulic conductivity in a soil with macropores. Soil Technol. 10, 115–131.

Marquardt, D.W., 1963. An algorithm for least-squares estimation of nonlinear parameters. SIAM J. Appl. Math. 11, 431–441.

Mayer, A.S., Huang, C., 1999. Development and application of a coupled-process parameter inversion model based on the maximum likelihood estimation method. Adv. Water Resour. 22, 841–853.

Medina, A., Carrera, J., 1996. Coupled estimation of flow and solute transport parameters. Water Resour. Res. 32, 3063–3076.

Mishra, S., Parker, J.C., 1989. Parameter estimation for coupled unsaturated flow and transport. Water Resour. Res. 25, 385–396.

Mohanty, B.P., Bowman, R.S., Hendrickx, J.M.H., van Genuchten, M.Th., 1997. New piecewise-continuous hydraulic functions for modeling preferential flow in an intermittent-flood-irrigated field. Water Resour. Res. 33, 2049–2063.

Mohanty, B.P., Bowman, R.S., Hendrickx, J.M.H., Šimůnek, J., van Genuchten, M.Th., 1998. Preferential transport of nitrate to a tile drain in an intermittent-flood-irrigated field: model development and experimental evaluation. Water Resour. Res. 34, 1061–1076.

Mualem, Y., 1976. A new model for predicting the hydraulic

conductivity of unsaturated porous media. Water Resour. Res. 12, 513–522.

Radcliffe, D.E., Tillotson, P.M., Hendrix, P.F., West, L.T., Box, J.E., Tollner, E.W., 1996. Anion transport in a piedmont ultisol: I. Field-scale parameters. Soil Sci. Soc. Am. J. 60, 755–761.

Reedy, O.C., Jardine, P.M., Wilson, G.V., Selim, H.M., 1996. Quantifying the diffusive mass transfer of nonreactive solutes in columns of fractured saprolite using flow interruption. Soil Sci. Soc. Am. J. 60, 1376–1384.

Roth, K., Jury, W.A., Flühler, H., Attinger, W., 1991. Transport of chloride through an unsaturated field soil. Water Resour. Res. 27, 2533–2541.

Schoen, R., Gaudet, J.P., Elrick, D.E., 1999. Modelling of solute transport in a large undisturbed lysimeter during steady-state water flux. J. Hydrol. 215, 82–93.

Schulin, R., van Genuchten, M.Th., Flühler, H., Ferlin, P., 1987. An experimental study of solute transport in a stony field soil. Water Resour. Res. 23, 1785–1794.

Šimůnek, J., Šejna, M., van Genuchten, M.Th., (1998). The HYDRUS-1D software package for simulating the one-dimensional movement of water, heat, and multiple solutes in variably-saturated media. Version 2.0, IGWMC-TPS-70, International Ground Water Modeling Center, Colorado School of Mines, Golden, Colorado, 202 pp.

Šimůnek, J., Wendroth, O., van Genuchten, M.Th., 1999. Estimating unsaturated soil hydraulic properties from laboratory tension disc infiltrometer experiments. Water Resour. Res. 35, 2965–2979.

Šimůnek, J., Jacques, D., Hopmans, J.W., Inoue, M., Flury, M., van Genuchten, M.Th., 2001. Solute transport during variably-saturated flow—inverse methods. In: Dane, J.H., Topp, G.C. (Eds.). Methods of Soil Analysis, Part 1, Physical Methods. 3rd ed. SSSA, Madison, WI in press.

Skopp, J., Gardner, W.R., 1992. Miscible displacement: an interacting flow region model. Soil Sci. Soc. Am. J. 56, 1680–1686.

Snow, V.O., Clothier, B.E., Scotter, D.R., White, R.E., 1994. Solute transport in a layered soil: experiments and modelling using the convection–disperion approach. J. Cont. Hydrol. 16, 339–358.

Steenhuis, T.S., Parlange, J.-Y., Andreini, M.S., 1990. A numerical model for preferential solute movement in structured soils. Geoderma 46, 193–208.

Sun, N.-Z., Yeh, W.W.-G., 1990. Coupled inverse problems in groundwater modeling. 1. Senstivity analysis and parameter identification. Water Resour. Res. 26, 2507–2525.

Vanderborght, J., 1997. Experimental and numerical study on non-reactive solute transport in soils. PhD no. 349, Faculteit Landbouwkundige en Toegepaste Biologische Wetenschappen, K.U. Leuven, Belgium, 310 pp.

Vanderborght, J., Vanclooster, M., Mallants, D., Diels, J., Feyen, J., 1996. Determining convective lognormal solute transport parameters from resident concentrations. Soil Sci. Soc. Am. J. 60, 1306–1317.

Vanderborght, J., Mallants, D., Vanclooster, M., Feyen, J., 1997. Parameter uncertainty in the mobile–immobile solute transport model. J. of Hydrol. 190, 75–101.

Vanderborght, J., Timmerman, A., Feyen, J., 2000. Solute transport for steady-state and transient flow in soils with and without macropores. Soil Sci. Soc. Am. J. 64, 1305–1317.

Vanderborght, J., Vanclooster, M., Timmerman, A., Mallants, D., Jacques, D., Hubrechts, L., Gonzalez, C., Feyen, J., Diels, J., Deckers, J., 2001. Overview of inert tracer experiments in key Belgian soil types: relation between transport, morphological and hydraulic soil properties. Water Resour. Res. in press.

van Genuchten, M.Th., 1980. A closed-form equation for predicting the hydraulic conductivity of unsaturated soils. Soil Sci. Soc. Am. J. 44, 892–898.

van Genuchten, M.Th., Wierenga, P.J., 1976. Mass transfer studies in sorbing porous media I. Analytical solutions. Soil Sci. Soc. Am. J. 40, 473–480.

van Genuchten, M.Th., Schaap, M.G., Mohanty, B.P., Šimůnek, J., Leij, F.J., 1999. Modeling flow and transport processes at the local scale. In: Feyen, J., Wiyo, K. (Eds.). Modelling of Transport Processes in Soils at Various Scales in Time and Space, pp. 23–45.

Ventrella, D., Mohanty, B.P., Šimůnek, J., Losavio, N., van Genuchten, M.Th., 2000. Water and chloride transport in a fine-textured soil: field experiments and modeling. Soil Sci. 165, 624–631.

Vogeler, I., Clothier, B.E., Green, S.R., Scotter, D.R., Tillman, R.W., 1996. Characterizing water and solute movement by time domain reflectometry and disk permeametry. Soil Sci. Soc. Am. J. 60, 5–12.

Wallach, R., Steenhuis, T.S., 1998. Model for nonreactive transport in structured soils with continuous preferential flow paths. Soil Sci. Soc. Am. J. 62, 881–886.

Zurmühl, T., Durner, W., 1996. Modeling transient water and solute transport in a biporous soil. Water Resour. Res. 32, 819–829.